Journal of Materials Chemistry A

Accepted Manuscript

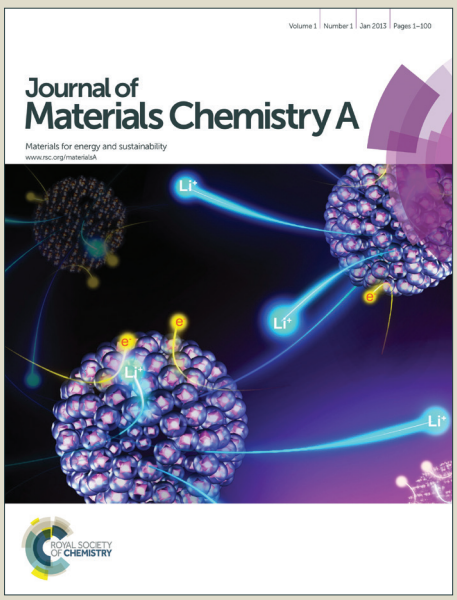

ROYAL SOCIETY OF CHEMISTRY

www.rsc.org/materialsA

Three-Dimensional Networked $NiCo_2O_4/MnO_2$ Branched Nanowire Heterostructure Arrays on Nickel Foam with Enhanced Supercapacitor Performance

Rujia Zou,[a,b] Muk Fung Yuen,[a] Zhenyu Zhang,[a] Junqing Hu,[b] Wenjun Zhang[a,*]

[a]Center of Super-Diamond and Advanced Films (COSDAF), Department of Physics and Materials Science, City University of Hong Kong, Hong Kong

E-mail: apwjzh@cityu.edu.hk

[b]State Key Laboratory for Modification of Chemical Fibers and Polymer Materials, College of Materials Science and Engineering, Donghua University, Shanghai 201620, China

Abstract

Networked branched nanowire heterostructure (BNH) hybrid material is a very promising structure for supercapacitor electrodes, which may provide enhanced electrochemical performance compared with electrodes comprising a single constituent or core/shell nanowire heterostructure counterparts. Herein, by using one-step hydrothermal reaction followed by a post-annealing treatment, we synthesized networked $NiCo_2O_4/MnO_2$ BNH arrays on Ni foam substrates and applied them as electrodes in supercapacitors. The as-prepared electrode exhibits ultrahigh specific capacitance, excellent rate capability, and superb cycling stability at a high charge/discharge current density. These outstanding overall electrochemical performances are attributed to the effective conductive transport path between component materials, reduced electron- and ion-transport pathways, enhanced surface area, and facile electrolyte infiltration into 3D networked BNH. The networked BNH design may provide a universal approach for the development of new electrode materials in high-performance psudocapacitors.

1. Introduction

With the great demand of energy consumption, there has been intensive research focusing on energy conversion from alternative energy sources and energy storage.[1,2] Supercapacitor is one of the most ideal candidates for energy storage because of its high power density, long lifespan, and safe operation.[3,4] In recent years, scientists have made great effort on the study of pseudocapacitors because their energy density associated with Faradaic reactions is substantially larger than that of electrical double-layer capacitors (EDLCs).[1-3] The performance of pseudocapacitors is largely determined by the characters of electrode materials. Among the various pseudocapacitor materials studied so far, transition metal oxides (MnO_2, NiO, V_2O_5, Co_3O_4, $NiCo_2O_4$ ect.) have shown great potentials, since they are low cost, environmentally friendly, naturally abundant, and can be fabricated using facile, cost-effective, and scalable techniques, such as hydro/solvothermal method and electrodeposition.[1-3] Generally, an ideal supercapacitor should have the merits of high specific capacitance and rate capability, and superb cycling stability.[1-4] However, pseudocapacitors fabricated with single-component nanomaterials or one-dimension (1D) nanomaterials as electrodes have been shown to have difficulties in satisfying all these requirements.[5-7] Therefore it is necessary to explore new nanostructured electrode materials to solve the problem . One possible solution is to develop three-dimensional (3D) heterostructured nanomaterials and grow them directly on electrode the 3D structures and the synergistic effects of component nanomaterials may lead to improved electrochemical performance of electrodes.[8-10]

3D core/shell heterostructure (CSH) nanowire arrays have enlarged surface area, effective transport pathway for charge carriers, and reduced “dead volume” from polymer binder, which are favorable for their electrode application in supercapacitors.[9-12] However, in the core/shell structure, the active sites of core nanowires are largely invalidated by the shell layer, which cannot fully utilize the electrochemical reactivity of the core nanowires. In contrast to CSH configuration, networked/branched nanowire heterostructures may not only

provide high-efficiency electron pathway for charge storage and delivery, but also effectively exploit the contribution of all constituents to the total capacitance.[13-15] For example, a branched nanowire heterostructure (BNH), in which core nanowires are featured with high specific capacitance, good electric conductivity, and high ion accessibility, and the branch nanowires have also the merits of high specific capacitance, short electron- and ion-transport pathways, and good electrolyte infiltration, would be promising for the further improvement of the overall performance of pseudocapacitors.

Ternary nickel cobaltite ($NiCo_2O_4$) and manganese dioxide (MnO_2) are two of the most widely investigated pseudocapacitive materials due to their high-theoretical gravimetric capacitance, and as well their low cost, natural abundance, environmental safety, and low toxicity.[16,17] In this work, using one-step hydrothermal reaction combined with a simple post annealing treatment, we synthesized networked $NiCo_2O_4/MnO_2$ BNH arrays directly on Ni foam substrates and evaluated their electrode performance for supercapacitors. Interestingly, the $NiCo_2O_4/MnO_2$ BNH arrays showed a specific capacitance of 2827 F g^{-1} at a current density of 2 mA cm^{-2}, which still maintained at 2339 F g^{-1} at 20 mA cm^{-2}. The electrode also presented excellent cycling stability with only 1.6% loss of specific capacity after 3000 cycles at a high charge/discharge current density. The impacts of the special geometric configuration of the BNH structure and the intrinsic characteristics of core and branch nanowires on the improvement of supercapacitive performance were demonstrated.

2. Experimental Section

Synthesis: The networked $NiCo_2O_4/MnO_2$ BNH arrays were synthesized on Ni foam using a one-step hydrothermal reaction followed with a simple post annealing process. All commercially available chemicals were used as received without further purification from Sinopharm Chemical Reagent Co. (Shanghai, China). In a typical synthesis, 0.15g of $Ni(NO_3)_2 \cdot 6H_2O$, 0.30g of $Co(NO_3)_2 \cdot 6H_2O$, and 1.00g urea were dissolved into a solution of

40 mL of H_2O at 50 ˚C to form a clear pink solution. The Ni foam substrates were immersed in a 2 M HCl solution for ~ 10 min to remove surface oxide layer, and then put into the Teflon autoclave. Then a solution of $Mn(NO_3)_2$ (50%) was dropwise added into Teflon autoclave under stirring, and maintained at 180 ˚C for 8 h. The Ni foam was taken out from autoclave after the solution was cooled down to room temperature, and then cleaned by ultrasonication in deionized water to remove the loosely attached products on its surface. Finally, the Ni foam substrate with loaded products was dried at 60 °C. In order to get crystallized $NiCo_2O_4/MnO_2$ BNH arrays on Ni foam, the samples were annealed at 300 °C in air for 2 h with a heating rate of 1 °C min.

$NiCo_2O_4@MnO_2$ CSH arrays on Ni foam were prepared by a two-step hydrothermal method. First, Mesoporous $NiCo_2O_4$ nanowires were synthesized through hydrothermal reaction and followed by thermal annealing process. In a typical synthesis procedure, a piece of nickel foam was cleaned with 2 M HCl solution, and then cleaned completely with deionized water and absolute ethanol. 1.185g of $CoCl_2·6H_2O$, 0.657g of $NiCl_2·6H_2O$, and 4.50g urea were dissolved into a solution of 40 mL of H_2O to form a clear pink solution. Ni foam was put in the solution in a 50 mL Teflon autoclave, and maintained at 140 ˚C for 8 h. After the solution was cooled down to room temperature, the Ni foam was taken out from solution was cleaned by ultrasonication to remove the loosely attached products on the surface in deionized water. And then, the Ni foams with the as-grown precursor were annealed in Ar gas at 300 °C for 2 h with a heating rate of 1 °C min. Second, the Ni foam was put again in a solution containing 0.03 M $KMnO_4$ in an autoclave, and was subsequently maintained at 160 ° C for 1 h. Finally, the sample was washed with distilled water, and annealed at 250 °C in air for 2 h to obtain $NiCo_2O_4@MnO_2$ CSH arrays.

Characterization: The samples were characterized with a D/max-2550 PC X-ray diffractometer (XRD; Rigaku, Cu-Ka radiation), a scanning electron microscope (SEM; S-4800), a transmission electron microscope (TEM; JEM-2100F) equipped with an energy

dispersive X-ray spectrometer (EDX), and an X-ray photoelectron spectrometer (ESCALab MKII) with an excitation source of Mg-K radiation.

Electrochemical measurements: The electrochemical performances of the as-synthesized materials were assessed on an Autolab (PGSTAT302N potentiostat) using a three-electrode mode in 1 M KOH solution. A platinum (Pt) plate and a saturated calomel electrode (SCE) were used as the counter and the reference electrodes, respectively. The nominal area of the Ni foam immersed into the electrolyte was controlled to be around 1 cm×1 cm. The mass loading of the networked $NiCo_2O_4/MnO_2$ BNH and $NiCo_2O_4@MnO_2$ CSH on Ni foam was ~ 0.92 mg cm^{-2} and ~ 1.06 mg cm^{-2}, respectively, after calcination.

3. Results and discussion

Fig. 1a shows the typical scanning electron microscopy (SEM) images of the networked $NiCo_2O_4/MnO_2$ precursor BNH synthesized by the one-step hydrothermal reaction. It can be seen that $NiCo_2O_4/MnO_2$ BNH arrays are grown uniformly on the Ni foam with a large area. The precursor BNH arrays are well aligned on the Ni foam with high quantity. The precursor BNH was easily converted to networked $NiCo_2O_4/MnO_2$ BNH through annealing process in air, as displayed in Fig. 1b. The vertically aligned $NiCo_2O_4$ nanowires serve as the cores or trunks in the BNHs, and they have a uniform length of ~ 5 μm with their diameter gradually shrinking from ~100 nm at bottom to ~20 nm at top. Interestingly, magnified SEM images (Figs. 1c and 1d) reveal that the ultrathin MnO_2 branched nanowires are grown directly on $NiCo_2O_4$ core nanowires, and the $NiCo_2O_4$ core nanowires are linked together by the MnO_2 branch nanowires, forming a networked heterostructure arrays. The networked $NiCo_2O_4/MnO_2$ BNH exhibit a hierarchical structure featured with open space between core and branched nanowires. This topological feature is beneficial for the electrolyte penetration, as discussed below. Cross-sectional SEM image of the sample in Fig. 1d further verifies that the ultrathin MnO_2 branch nanowires are distributed quite uniformly on the whole $NiCo_2O_4$

core nanowires and the length of the MnO_2 nanowires gradually increases from ~50 nm at the trunk bottom to ~500 nm at the trunk top.

X-ray photoelectron spectroscopy (XPS) was employed to confirm the chemical composition of the samples, as illustrated in Fig. 1e and Fig. S1. The peak located at 529.7 eV is assigned to O element in oxide.[18] As shown in the inset, the Mn $2p_{3/2}$ and Mn $2p_{1/2}$ peaks centered at 642.3 eV and 653.9 eV, respectively, have a spin-energy separation of 11.6 eV, which are in accordance with previous data observed in MnO_2.[19, 20] The Co 2p peak is fitted by two spin-orbit characteristics of Co^{2+} and Co^{3+} (Fig. S1a), and the Ni 2p spectrum can also be deconvoluted with two spin-orbit characteristics of Ni^{2+} and Ni^{3+} (Fig. S1b), which agree well with the previous research on $NiCo_2O_4$.[21,22] Fig. S2 shows XRD pattern of the networked $NiCo_2O_4/MnO_2$ BNH after calcination (denoted as (i)) with reference to the standard diffractions spectra of $NiCo_2O_4$ (Joint Committee on Powder Diffraction Standards (JCPDS) card No. 20-0781) and MnO_2 (JCPDS No. 12-0141). It is obvious that all the diffraction peaks from the sample can be indexed to the $NiCo_2O_4$ and MnO_2.

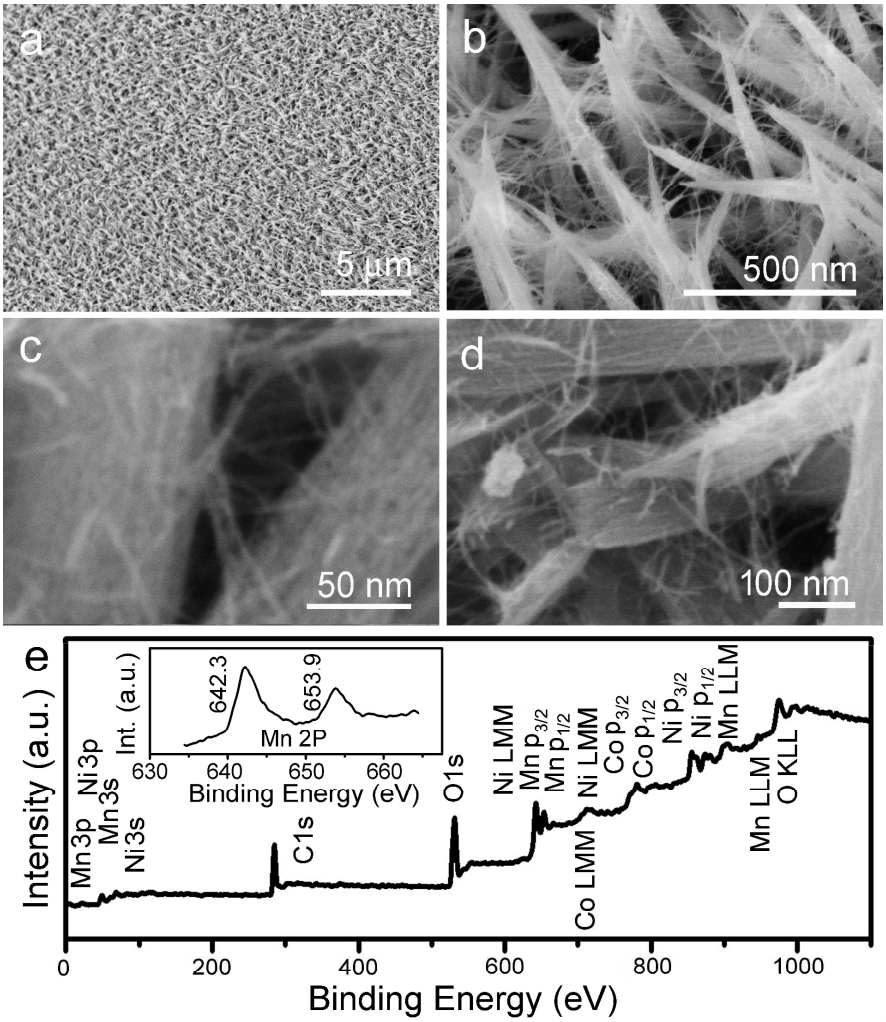

Fig. 1 (a) As-synthesized networked $NiCo_2O_4/MnO_2$-precursor BNH arrays on Ni foam. (b) Networked $NiCo_2O_4/MnO_2$ BNH arrays on Ni foam. (c) The plain and (d) cross-sectional views of magnified SEM images of networked $NiCo_2O_4/MnO_2$ BNH arrays on Ni foam. (e) XPS spectrum of the networked $NiCo_2O_4/MnO_2$ BNH. The inset is the high-resolution Mn 2p spectrum.

The microstructure of the networked $NiCo_2O_4/MnO_2$ BNH was further investigated by using TEM. Similar to the SEM observations above, the low-magnification TEM image in Fig. 2a shows that a large number of MnO_2 branch nanowires are assembled on the $NiCo_2O_4$ core nanowires, and the $NiCo_2O_4$ core nanowires are linked by the MnO_2 branch nanowires to

form a network structure. The ultrathin MnO_2 branch nanowires have a diameter of ~5 nm. Besides, the TEM images reveal that $NiCo_2O_4$ core nanowires are mesoporous with the pore size ranging from 2 to 10 nm. The formation of mesoporous structure is considered to be due to the release of H_2O and gases by the decomposition/oxidation of intermediates during annealing. The N_2 adsorption/desorption isotherm curve and the corresponding pore size distribution plot also support the porous nature of $NiCo_2O_4$ nanowires, as shown in Fig. S3. The Brunauer-Emmett-Teller (BET) surface area is ~45 m^2/g; and the average pore size is about 7.4 nm, which coincides with the TEM observation in Fig. 2b. Moreover, the MnO_2 branch nanowires root on two $NiCo_2O_4$ nanowires to form the heterojunctions (marked by blue arrows), suggesting that the MnO_2 branch nanowires are not just physically attached to the surfaces of $NiCo_2O_4$ core nanowires. As seen from the high-resolution TEM (HRTEM) image in Fig. 2c, the lattice fringes spaced by 0.24 nm in core nanowires are attributed to the (220) planes of $NiCo_2O_4$ crystal, and the fringes spaced by 0.28 nm in branch nanowires correspond to the (001) planes of MnO_2. The observations agree well with that reported for the $NiCo_2O_4$ and MnO_2 nanomaterials.[3,23] EDS spectra collected at the selected areas are depicted in Fig. 2d (at junction area as denoted by the blue hoop) and Fig. S4 (for $NiCo_2O_4$ core and MnO_2 branch nanowires separately). The EDX analysis of the sample clearly demonstrates the presence of Co, Ni, and O elements in networked BNH structure where Co, Ni, Mn and O elements are in core nanowire and Mn and O elements are in branch nanowires.

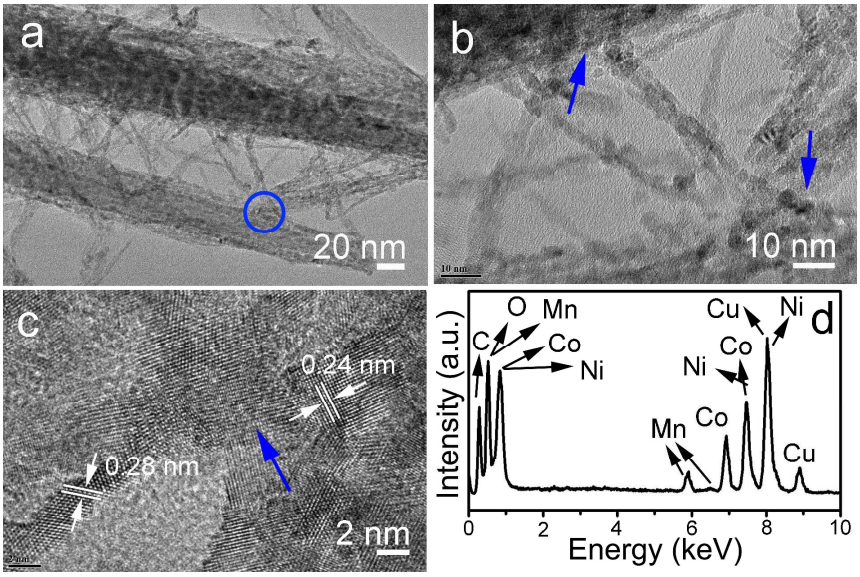

Fig. 2 (a) and (b) TEM images of the networked $NiCo_2O_4/MnO_2$ BNHs. (c) HRTEM image of the networked $NiCo_2O_4/MnO_2$ BNH. (d) EDS pattern collected on the selected junction area of networked $NiCo_2O_4/MnO_2$ BNH as denoted by the blue hoop. The Cu and C signals originate from the TEM grid.

To the best of our knowledge, there has been no report on networked 3D BNH arrays directly grown on conductive substrates *via* one-step hydrothermal method. In order to understand the formation process of the networked $NiCo_2O_4/MnO_2$ BNH, the morphology evolution of samples was investigated at the different reaction stages of hydrothermal process. The SEM images of the samples after reaction for 1, 4, and 8 h (other reaction conditions were kept the same) are presented in Figs. 3a-c, respectively. Only NiCo-precursor (Ni_xCo_{2x}•$(OH)_{6x}$) core nanowire array could be observed on Ni foam after reaction for 1 h (Fig. 3a and Fig. S5), and the vertically aligned NiCo-precursor nanowires have a uniform length. As reaction went on for 4 h (Fig. 3b), some MnO_2-precursor branch nanowires were grown on the NiCo-precursor core nanowires. Further prolonging the reaction to 8 h, Mn-precursor nanowires bridged NiCo-precursor nanowires, resulting in a BNH network (Fig. 3c). After annealing, the networked $NiCo_2O_4/MnO_2$ BNH arrays were obtained on Ni foam (Fig.

3d). Based on these observations, a possible growth mechanism for the networked $NiCo_2O_4/MnO_2$ BNH arrays on Ni foam is proposed as following, and as shown schematically in Fig. 3e. First, the precursor compounds were formed by the reaction between metal cations (Co^{2+}, Ni^{2+} and Mn^{2+}) and OH^- anions released from hydrolysis of urea in aqueous solution.[24] Due to easy and rapid self-assembly of Co^{2+}, Ni^{2+} and OH^-,[16] the vertically aligned NiCo-precursor nanowires have the priority to grow on Ni foam (Fig. 3a). Second, similar to the selective growth of many other nanomaterials on graphite oxide (GO) sheets,[25-27] the interaction between OH^- groups adsorbed on NiCo-precursor core nanowires and Mn^{2+} initiates the selective growth of Mn-precursor nanowires in a suitable solvent environment. In this process, the OH^- anions on the NiCo-precursor function as nucleation sites for the Mn^{2+} ions which further bond with OH^- anions; the repeated reactions leads to the growth of Mn-precursor nanowires. With the further prolonged reaction time, Mn-precursor nanowires grow longer and reach the nearby NiCo-precursor core nanowires. Due to the excess OH^- groups on the surfaces of other NiCo-precursor nanowires, the Mn-precursor nanowires will be anchored on another NiCo-precursor core nanowire, forming a networked architecture.

According to previous studies on BNH, the size of the nanocrystal seeds on core nanowire has a strong impact on the diameter of the branch nanorods/nanowires grown on the core nanowire,[27,28] i.e., by controlling the size of nanocrystal seeds, the diameter of branch nanorods/noawires can be tuned. In this work we obtained ultrathin branch nanowires by employing the interaction between OH^- groups and Mn^{2+}, which benefits their electrochemical applications. In Table S1, we briefly summarize the fabrication method reported thus far for growing different BNHs, e.g., solution growth on pre-formed nanowires,[29-31] sequential catalyst assisted growth,[32,33] and one-step self-catalyzed growth.[34,35] Compared with these methods, our approach utilizes one-step hydrothermal reaction followed by post annealing treatment to grow BNHs, and thus it has the advantages in simplifying

synthesis procedure, avoiding toxic gaseous precursors and byproducts, low reaction temperature, and no residual metal catalyst impurities in the product.

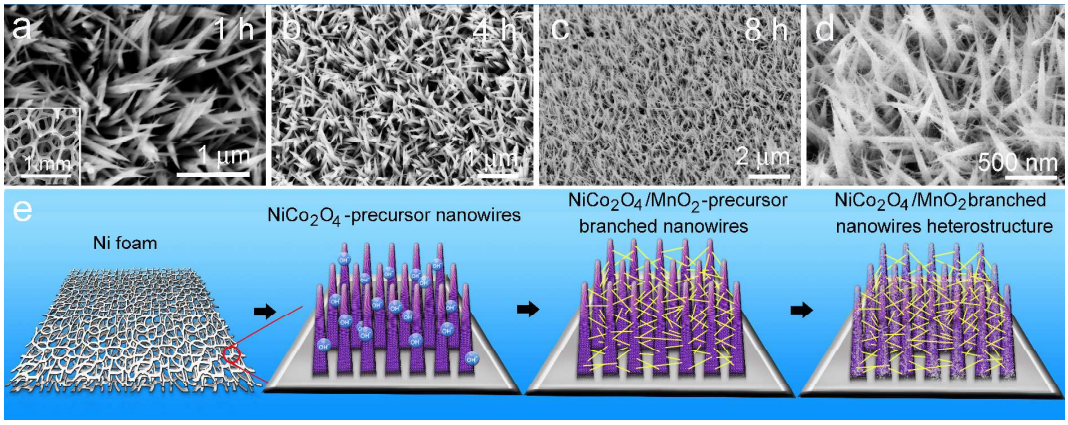

Fig. 3 (a-c) SEM morphologies of the samples taken after reaction for : (a) 1 h, (b) 4 h, (c) 8 h, respectively. (d) SEM image of the networked $NiCo_2O_4/MnO_2$ BNH arrays on Ni foam after hydrothermal reaction for 8 h and post annealing treatment. (e) Schematic illustration of the formation of networked $NiCo_2O_4/MnO_2$ BNH arrays on Ni foam.

The electrochemical properties of networked $NiCo_2O_4/MnO_2$ BNH, $NiCo_2O_4@MnO_2$ CSH (Fig. S6), and $NiCo_2O_4$ nanowires (Fig. S7) electrodes were studies in a standard three-electrode configuration using 1.0 M KOH electrolyte. Figure 4a shows the cyclic voltammetry (CV) curves of the networked $NiCo_2O_4/MnO_2$ BNH electrode at different scan rates of 5, 20, 50, and 100 mV s^{-1} in the potential window of 0 to 0.6 V. The shapes of the CV curves clearly confirm the pseudocapacitive characteristics of the networked $NiCo_2O_4/MnO_2$ BNH, which is different from EDLCs featured with nearly rectangular CV curves. The redox peaks were observed in all CV curves, which are mainly caused by the Faradaic redox reactions related to M-O/M-O-ON, where M refers to Mn, Co or Ni ions, N refers to K or H ions.[23] The redox current increased as the scan rate increased from 5 to 100 mV s^{-1}, and the oxidation and reduction peaks shifted toward higher and lower potentials, respectively, with a large potential

separation. However, the shapes of these CV curves did not change obviously, suggesting that the electrode enabled excellent electrochemical reversibility and high rate capability. Fig. S8 shows the CV curves of the networked $NiCo_2O_4/MnO_2$ BNH, networked $NiCo_2O_4@MnO_2$ BNH with reaction time of 4 h, and $NiCo_2O_4$ nanowires electrodes at a scan rate of 10 mV s^{-1}. It is obvious that the shapes of these CV curves are different, which is attributed to the additional pseudocapacitance contributed by the MnO_2 branch nanowires. Galvanostatic charge-discharge (CD) measurement is a more accurate technique for pseudocapacitances analysis.[36-38] In this work, the galvanostatic CD tests were conducted in a potential window between 0 and 0. 50 V at various discharge current densities ranging from 2 to 100 mA cm^{-2}, as shown in Fig. 4b and Fig. S9. The specific capacitance of the networked $NiCo_2O_4/MnO_2$ BNH electrode was calculated to be 2827, 2687, 2532, 2504, 2413, 2339, 2211, 2163, 1891 F g^{-1} at current densities of 2, 5, 8, 10, 15, 20, 30, 50, and 100 mA cm^{-2}, respectively, as shown in Fig. 4c (red curve). Significantly, at the high current density of 100 mA cm^{-2}, the specific capacitance could still be maintained at a high value of 1891 F g^{-1}. The capacitance of BNH electrode is higher than those of $NiCo_2O_4@MnO_2$ CSH electrode (2572 and 758 F g^{-1} at current densities of 2 and 100 mA cm^{-2}) (Fig. 4c, blue curve) and $NiCo_2O_4$ nanowire arrays (Fig. 4c, green curve). Moreover, it is also much higher than the previously reported capacitance values of $NiCo_2O_4$ nanowire arrays[23,36-40] and composite electrode materials of CSH electrodes, such as $NiCo_2O_4@MnO_2$ CSH,[41] $NiCo_2O_4@NiO$ CSH,[42] Co_3O_4 $@MnO_2$ CSH,[43] CoO@NiHON CSH,[44] and $Ni_3S_2@Ni(OH)_2$ CSH.[8]

As we know, good rate capability is a very important requirement for supercapacitors. As shown in Fig. 4c, the specific capacitance of networked $NiCo_2O_4/MnO_2$ BNH electrode could be retained at about 82.6% when the discharge current density increased from at 2 mA cm^{-2} to 20 mA cm^{-2}, and it was still at ~ 66.8% even when the discharge current density increased to 100 mA cm^{-2}, which are much better than pure $NiCo_2O_4$ nanomaterials, hybrid $NiCo_2O_4$-based nanomaterials and pure metal oxides nanomaterials.[36-44] A long cycle life at high current

densities is also required for supercapacitors for actual application. The cycling stability of networked $NiCo_2O_4/MnO_2$ BNH electrode was evaluated by the repeated CD measurement at high current densities of 10 mA cm^{-2}, as shown in Fig. 4d. The inset of Fig. 4d shows first few cycles of charge-discharge curves. Interestingly, the specific capacitance gradually decreased from 2504.6 F g^{-1} for the first cycle to 2465.7 F g^{-1} after 3000 cycles, deriving an overall capacitance loss of only ~1.6 %. This cyclic performance is superior to those of $NiCo_2O_4@MnO_2$ CSH and $NiCo_2O_4$ nanowire electrodes (Fig. S10) and is also better than that of $NiCo_2O_4$ nanowire array on Ni foam.[36-44]

The morphology of the $NiCo_2O_4/MnO_2$ BNH after 3000 charge/discharge cycles at constant current density of 10 mA cm^{-2} was characterized by SEM and TEM, as shown in Fig. S11. The electrode of $NiCo_2O_4/MnO_2$ BNH could almost preserve its structural integrity, except for the increased roughness on the electrode surface, some expansion, and slightly fracturing of branch nanowires caused by the redox reactions during the repeated charge/discharge processes. Moreover, it was also noted that the specific capacitances of $NiCo_2O_4@MnO_2$ CSH and $NiCo_2O_4$ nanowire electrodes gradually increased to their maxima and started to decrease, which is believed to be due to the slow activation of active electrode materials as in previous reports.[28,45] In contrast to that, the specific capacitance of networked $NiCo_2O_4/MnO_2$ BNH electrode showed only monotonic and slow decrease during cyclic test, indicating that BNH is much easier to be activated. Finally, by comparing with the electrochemical properties of the networked $NiCo_2O_4/MnO_2$ BNH electrode synthesized by reaction for 4 h (red curve) and the $NiCo_2O_4$ nanowire electrode (green curve), it is found that the specific capacitance and rate capability of the former is much better than the latter one, as shown in Fig. 4c. It further verifies that the MnO_2 branch also make non-neglectable contribution to the electrochemical performance of the BNH.

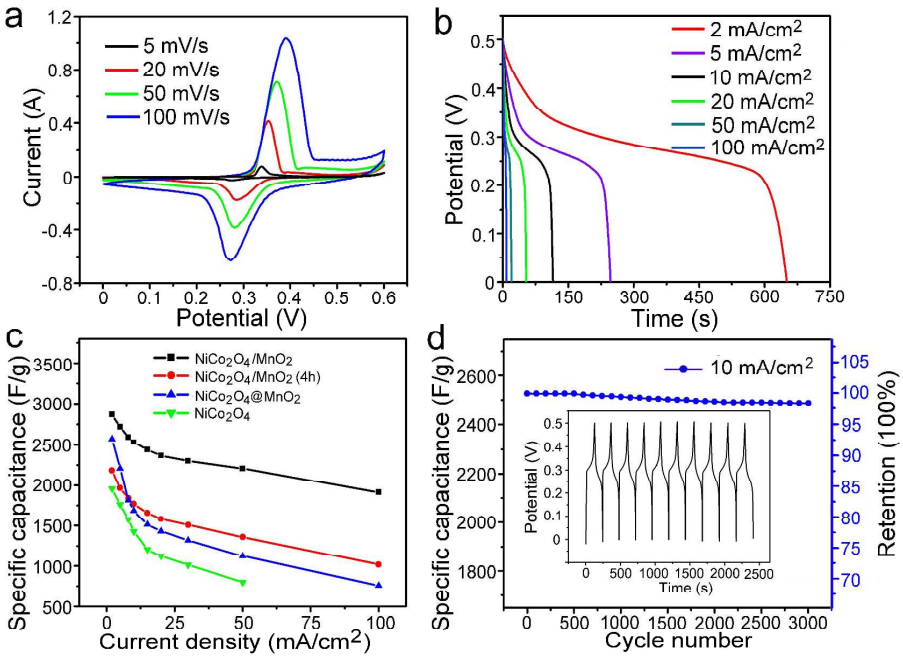

Fig. 4 (a) CV curves at different scan rates recorded from the networked $NiCo_2O_4/MnO_2$ BNH electrode. (b) Discharge curves of the networked $NiCo_2O_4/MnO_2$ BNH electrode. (c) Specific capacitances of networked $NiCo_2O_4/MnO_2$ BNH, networked $NiCo_2O_4/MnO_2$ BNH (4 h reaction), $NiCo_2O_4$@MnO_2 CSH and $NiCo_2O_4$ nanowires electrodes at different current densities. (d) Cycling performanc of networked $NiCo_2O_4/MnO_2$ BNH electrode during 3000 cycles at constant current densities of 10 mA cm^{-2}. The inset shows the first few cycles of charge-discharge curves.

Based on the above measurements, the electrode of networked $NiCo_2O_4/MnO_2$ BNH arrays on Ni foam showed excellent electrochemical performance, including high specific capacitance, excellent rate capability, and long cycling stability, which is superior to other electrode materials based on $NiCo_2O_4$ and its composite (Table 1).[8,23,36-44] The special geometric configuration and synergistic effects from each component of the networked $NiCo_2O_4/MnO_2$ BNH are believed to be the key for the enhanced electrochemical performance. (1) The mesoporous $NiCo_2O_4$ core nanowires with porous size in the range of 2-10 nm and well separated ultrathin MnO_2 branched nanowires with diameters of about 5 nm

largely increase the amount of electroactive sites. (2) The networked BNH may provide high-efficiency electron "superhighways" for charge storage and delivery, which could also give effective electrons transport between MnO_2 and $NiCo_2O_4$ nanowires. (3) The 3D BNH arrays have a large amount of open channels, exposing both MnO_2 branch nanowires and $NiCo_2O_4$ core nanowires fully to the electrolyte, and thus providing enlarged electrode/electrolyte contact area. (4) Both $NiCo_2O_4$ and MnO_2 are good pseudocapacitor materials, the combination of these two components provides a strong synergistic effect. In the 3D BNH, the $NiCo_2O_4$ core nanowires can be easily accessed by OH^-, which enhance the redox reactions. It is also noteworthy that the porous structure of $NiCo_2O_4$ core nanowires could further increase the electrolyte-material contact area, which is favorable for high-power energy storage. In contrast, in the core-shell hybrid nanostructures in electrode systems, the active sites of core materials were largely hindered by shell. Finally, the direct growth of MnO_2 branch nanowires on highly conductive $NiCo_2O_4$ core nanowires on metal Ni substrate can reduce charge transfer barrier between these materials, and ensure good mechanical adhesion as well. All these prominent features of the networked $NiCo_2O_4/MnO_2$ BNH lead to its outstanding overall electrode performance in supercapacitors.

Table 1. Electrochemical performance of the networked $NiCo_2O_4/MnO_2$ BNH in comparison with electrodes based on different $NiCo_2O_4$ nanostructures and their composites reported in literature.

Type of materials	Specific capacitance	Rate capability	Cycling stability	Refs.
$NiCo_2O_4$ nanosheets/Ni foam	1450 F g^{-1} at 20 A g^{-1}	72 % from 2 to 20 A g^{-1}	6 % after 2400 cycles	36
Mesoporous $NiCo_2O4$ nanosheets/Ni foam	1708 F g^{-1}/2.05 F cm^{-2} at 19.8 mA cm^{-2}	59 % from 1.8 to 19.8 mA cm^{-2}	6.7 % after 3000 cycles	37
$NiCo_2O_4$ nanorods/carbon fibers	500 F g^{-1} at 20 A g^{-1}	49 % from 1 to 20 A g^{-1}	8.5 % after 3000 cycles	38
$NiCo_2O_4$ microsphere assembled by nanowires	532 F g^{-1} at 20 A g^{-1}	70 % from 1 to 20 A g^{-1}	19 % after 3000 cycles	23

Hierarchical $NiCo_2O_4$	1072 F g^{-1} at 10 A g^{-1}	58 % from 1 to 20 A g^{-1}		39
Chain-like $NiCo_2O_4$ nanowires	986 F g^{-1} at 20 A g^{-1}	77 % from 2 to 20 A g^{-1}	2.5 % after 3000 cycles	40
Graphene/MnO_2/PEDOT:PSS	380 F g^{-1} at 0.1 mA cm^{-2}	70 % from 0.5 to 5 mA cm^{-2}	7 % after 3000 cycles	46
Co_3O_4 NW@MnO_2 NS	480 F g^{-1} at 2.67 A g^{-1}	56% from 4 to 44.7 mA cm^{-2}	2.7 % after 5000 cycles	43
Ni_3S_2 NW@$Ni(OH)_2$ NS	1037.5 F g^{-1} at 2.67 A g^{-1}		0.9 % after 2000 cycles	8
NiO/$NiCo_2O_4$/Co_3O_4 composite	1600 F g^{-1} at 5 mA cm^{-2}	75.5 % from 5 to 50 mA cm^{-2}	5.1 % after 1000 cycles	47
$NiCo_2O_4$ NW@MnO_2 NF	1471.4 F g^{-1}/1.66 F cm^{-2} at 20 mA cm^{-2}		12 % after 2000 cycles	41
networked $NiCo_2O_4$/MnO_2 BNH	2339 F g^{-1} at 20 mA cm^{-2} (22 A g^{-1})	82.6 % from 2 to 20 mA cm^{-2} 76.4 % from 2 to 50 mA cm^{-2}	1.6 % after 3000 cycles	This work

4. Conclusion

In summary, we have successfully fabricated a 3D electrode by directly growing networked $NiCo_2O_4$/MnO_2 BNH arrays on Ni foam using a one-step hydrothermal reaction followed with a simple post annealing treatment. The $NiCo_2O_4$/MnO_2 BNH electrode show excellent electrochemical performance, such as ultrahigh specific capacitances of 2827 and 2163 F g^{-1} at current densities of 2 and 50 mA cm^{-2}, respectively, excellent rate capability; long cycling stability with a capacitance loss of 1.6 % after 3000 cycles. These outstanding overall electrochemical performances are attributed to the effective conductive transport path between component materials, reduced electron- and ion-transport pathways, enhanced surface area, and facile electrolyte infiltration into 3D networked BNH. The 3D networked BNH design may be applied for the development of new electrode materials for high-performance supercapacitors.

Acknowledgements

This work was financially supported by the National Natural Science Foundation of China (Grant No. 51302035), the Project funded by China Postdoctoral Science Foundation, the Science and Technology Commission of Shanghai Municipality (Grant No. 13ZR1451200),

the PhD Programs Foundation of the Ministry of Education of China (Grant No. 20130075120001), and the Fundamental Research Funds for the Central Universities.

Reference:

1 G. P. Wang, L. Zhang and J. J. Zhang, *Chem. Soc. Rev.*, 2012, **41**, 797.

2 J. Jiang, Y. Y. Li, J. P. Liu, X. T. Huang, C. Z. Yuan and X. W. Lou, *Adv. Mater.*, 2012, **24**, 5166.

3 X. Y. Lang, A. Hirata, T. Fujita and M. W. Chen, *Nat. Nanotechnol.*, 2011, **6**, 232.

4 M. F. El-Kady, V. Strong, S. Dubin and R. B. Kaner, *Science*, 2012, **335**, 1326.

5 L. Q. Mai, F. Dong, X. Xu, Y. Z. Luo, Q. Y. An, Y. L. Zhao, J. Pan and J. N. Yang, *Nano Lett.*, 2013, **13**, 740.

6 J. X. Zhu, L. J. Cao, Y. S. Wu, Y. J. Gong, Z. Liu, H. E. Hoster, Y. H. Zhang, S. T. Zhang, S. B. Yang and Q. Y. Yan, *Nano Lett.*, 2013, **13**, 5408.

7 Z. N. Yu, B. Duong, D. Abbitt and J. Thomas, *Adv. Mater.*, 2013, **25**, 3302.

8 W. J. Zhou, X. H. Cao, Z. Y. Zeng, W. H. Shi, Y. Y. Zhu, Q. Y. Yan, H. Liu, J. Y. Wang and H. Zhang, *Energy Environ. Sci.*, 2013, **6**, 2216.

9 X. H. Lu, T. Zhai, X. H. Zhang, Y. Q. Shen, L. Y. Yuan, B. Hu, L. Gong, J. Chen, Y. H. Gao, J. Zhou, Y. X. Tong and Z. L. Wang, *Adv. Mater.*, 2012, **24**, 938.

10 C. Guan, X. L. Li, Z. L. Wang, X. H. Cao, C. Soci, H. Zhang and H. J. Fan, *Adv. Mater.*, 2012, **24**, 4186.

11 C. Zhou, Y. W. Zhang, Y. Y. Li, J. P. Liu, *Nano Lett.*, 2013, **13**, 2078.

12 J. Xu, Q. F Wang, X. W. Wang, Q. Y. Xiang, B. Liang, D. Chen and G. Z. Shen, *ACS Nano*, 2013, **7**, 5453.

13 L. Q. Mai, F. Yang, Y. L. Zhao, X. Xu, L. Xu and Y. Z. Luo, *Nat. Commun.*, 2011, **2**, 381.

14 C. Cheng and H. J. Fan, *Nano Today*, 2012, **7**, 327.

15 C. Liu, J. Y. Tang, H. M. Chen, B. Liu and P. D. Yang, *Nano Lett.*, 2013, **13**, 2989.

16 L. Huang, D. C. Chen, Y. Ding, S. Feng, Z. L. Wang and M. L. Liu, *Nano Lett.*, 2013, **13**, 3135.

17 W. F. Wei, X. W. Cui, W. X. Chen and D. G. Ivey, *Chem. Soc. Rev.*, 2011, **40**, 1697.

18 H. Xia, M. O. Lai and L. Lu, *J. Mater. Chem.*, 2010, **20**, 6896.

19 M. Toupin, T. Brousse and D. Belanger, *Chem. Mater.*, 2004, **16**, 3184.

20 M. Chigane and M. Ishikawa, *J. Electrochem. Soc.*, 2000, **147**, 2246.

21 J. F. Marco, J. R. Gancedo, M. Gracia, J. L. Gautier, E. I. Ríos, H. M. Palmer, C. Greavesc and F. J. Berry, *J. Mater. Chem.*, 2001, **11**, 3087.

22 B. Cui, H. Lin, Y. Z. Liu, J. B. Li, P. Sun, X. C. Zhao and C. J. Liu, *J. Phys. Chem. C*, 2009, **113**, 14083.

23 H. L. Wang, Q. M. Gao and L. Jiang, *Small*, 2011, **7**, 2454.

24 Q. F. Wang, X. F. Wang, J. Xu, X. Ouyanga, X. J. Hou, D. Chen, R. M. Wang and G. Z. Shen, *Nano Energy*, 2014, **8**, 44.

25 H. L. Wang, J. T. Robinson, G. Diankov and H. J. Dai, *J. Am. Chem. Soc.*, 2010, **132**, 3270.

26 H. L. Wang, L. F. Cui, Y. Yang, H. S. Casalongue, J. T. Robinson, Y. Y. Liang, Y. Cui and H. J. Dai, *J. Am. Chem. Soc.*, 2010, **132**, 13978.

27 R. J. Zou, Z. Y. Zhang, L. Yu, Q. W. Tian, Z. G. Chen and J. Q. Hu, *Chem - Eur. J.,* 2011, **17**, 13912.

28 Z. Rujia, Z. Y. Zhang, L. Jiang, K. B. Xu, Q. W. Tian, S. L. Xue, J. Q. Hu, Y. Bando and D. Golberg, *J. Mater. Chem.*, 2012, **22**, 19196.

29 C. W. Cheng, B. Liu, H. Y. Yang, W. W. Zhou, L. Sun, R. Chen, S. F. Yu, J. X. Zhang, H. Gong, H. D. Sun and H. J. Fan, *ACS Nano*, 2009, **3**, 3069.

30 W. Zhou, C. Cheng, J. P. Liu, Y. Y. Tay, J. Jiang, X. T. Jia, J. X. Zhang, H. Gong, H. H. Hng, T. Yu and H. J. Fan, *Adv. Funct. Mater.*, 2011, **21**, 2439.

31 A. Kargar, Y. Jing, S. J. Kim, C. T. Riley, X. Q. Pan and D. L. Wang, *ACS Nano*, 2013, **7**, 11112.

32 D. Wang, F. Qian, C. Yang, Z. H. Zhong and C. M. Lieber, *Nano Lett.*, 2004, **4**, 871.

33 C. Yan, X. Li, K. Zhou, A. Pan, P. Werner, S. L. Mensah, A. T. Vogel and V. Schmidt, *Nano Lett.*, 2012, **12**, 1799.

34 J. Y. Lao, J. G. Wen and Z. F. Ren, *Nano Lett.,* 2002, **2**, 1287.

35 F. Sauvage, F. Di Fonzo, A. L. Bassi, C. S. Casari, V. Russo, G. Divitini, C. Ducati, C. E. Bottani, P. Comte and M. Graetzel, *Nano Lett.*, 2010, **10**, 2562.

36 C. Z. Yuan, J. Y. Li, L. R. Hou, X. G. Zhang, L. F. Shen and X. W. Lou, *Adv. Funct. Mater.*, 2012, **22**, 4592.

37 G. Q. Zhang and X. W. Lou, *Adv. Mater.*, 2013, **25**, 976.

38 G. Zhang and W. X. Lou, *Sci. Rep.*, 2013, **3**, 1470.

39 J. Chang, J. Sun, C. H. Xu, H. Xu and L. Gao, *Nanoscale*, 2012, **4**, 6786.

40 R. J. Zou, K. B. Xu, T. Wang, G. J. He, Q. Liu, X. J. Liu, Z. Y. Zhang and J. Q. Hu, *J. Mater. Chem. A*, 2013, **1**, 8560.

41 L. Yu, G. Q. Zhang, C. Z. Yuan and X. W. Lou, *Chem. Commun.*, 2013, **49**, 137.

42 W. L. Yang, Z. Gao, J. Ma, X. M. Zhang, J. Wang and J. Y. Liu, *J. Mater. Chem. A*, 2014, **2**, 1448.

43 J. P. Liu, J. Jiang, C. W. Cheng, H. X. Li, J. X. Zhang, H. Gong and H. J. Fan, *Adv. Mater.*, 2011, **23**, 2076.

44 C. Guan, J. P. Liu, C. W. Cheng, H. X. Li, X. L. Li, W. W. Zhou, H. Zhang and H. J. Fan, *Energy Environ. Sci.*, 2011, **4**, 4496.

45 X. H. Lu, D. Z. Zheng, T. Zhai, Z. Q. Liu, Y. Y. Huang, S. L. Xie and Y. X. Tong, *Energy Environ. Sci.*, 2011, **4**, 2915.

46 G. H. Yu, L. B. Hu, N. Liu, H. L. Wang, M. Vosgueritchian, Y. Yang, Y. Cui and Z. A. Bao, *Nano Lett.*, 2011, **11**, 4438.

47 M. C. Liu, L. B. Kong, C. Lu, X. M. Li, Y. C. Luo and L. Kang, *ACS Appl. Mater. Interfaces*, 2012, **4**, 4631.

The table of contents entry

Three-dimensional networked $NiCo_2O_4/MnO_2$ branched nanowire heterostrure arrays directly grown on Ni foam for high-performance electrode application in supercapacitors.

Figure for contents entry only